ELSEVIER

Journal of Alloys and Compounds 403 (2005) 154–160

Journal of ALLOYS AND COMPOUNDS

www.elsevier.com/locate/jallcom

Damping characteristics of a $Ti_{40.5}Ni_{49.5}Zr_{10}$ shape memory alloy

S.F. Hsieh [a], S.K. Wu [b,*]

[a] *Department of Mold and Die Engineering, National Kaohsiung University of Applied Science, Kaohsiung, Taiwan 807, Republic of China*
[b] *Department of Materials Science and Engineering, National Taiwan University, Taipei, Taiwan 106, Republic of China*

Received 12 April 2005; accepted 27 April 2005
Available online 14 July 2005

Abstract

$Ti_{40.5}Ni_{49.5}Zr_{10}$ alloy undergoes B2 ↔ B19′ martensitic transformation. Damping capacities of B19′ and B2 phases of this alloy are lower than those of $Ti_{51}Ni_{49}$ alloy due to Zr atoms solid-soluted hardening. Transformation temperatures of this alloy decrease, but transformation peak heights Q^{-1}_{max} increase with increasing aging time at 300 °C due to the formation of finer $(0\,0\,1)_M$ twins for specimens aged longer. The Q^{-1}_{max} peaks of the slightly cold-rolled $Ti_{40.5}Ni_{49.5}Zr_{10}$ alloy are higher than those of the as-annealed alloy, which may be because the thinner twins are induced by small deformation.

Keywords: Shape memory alloy; Damping capacity; Martensitic transformation; Aging; Cold-rolling

1. Introduction

Near-equiatomic TiNi shape memory alloys (SMAs) are technologically important due to their superior shape memory effect and superelastic properties. However, the applications of these alloys are limited to use at temperatures lower than 100 °C because their starting temperatures of martensitic transformation, Ms, are usually lower than 60 °C. High temperature SMAs with Ms temperatures higher than 100 °C have been exhaustively researched due to their many potential applications. In particular, the TiNiZr and TiNiHf ternary high temperature SMAs have been developed with high Ms temperatures [1–3].

In addition to shape memory effect and superelastic properties, TiNi SMAs have also been found to exhibit high mechanical damping capacity [4]. Damping mechanisms, in general, involve the stress-induced movement of defects. For high-damping metals, the major mechanisms are either stress-induced movement of dislocations or planar defects [5], and most of these mechanisms can be phenomenologically split into three classes: dynamic hysteresis, static hysteresis and transformation mechanisms. Dynamic hysteresis is produced by stress-aided ordering of defects overcoming local barriers by thermal activation and it yields damping that is frequency-dependent and amplitude-independent. Static hysteresis appears due to the stress-induced 'unpinning' or 'break-away' process of the defects [5–7] and it yields damping that is frequency-independent and amplitude-dependent. Some metals exhibit a high level of damping in the transformation region, for example, thermoelastic martensitic transformation of SMAs [8,9]. Such thermoelastic damping is frequently amplitude-independent and is proportional to the transformation rate. In the present study, the characteristics of internal friction (IF) in a $Ti_{40.5}Ni_{49.5}Zr_{10}$ SMA are investigated. In addition, the effect of aging and cold-rolling on the damping capacity of this alloy is also discussed.

2. Experimental procedure

The conventional tungsten arc melting technique was employed to prepare $Ti_{40.5}Ni_{49.5}Zr_{10}$ (in at.%) alloy. Titanium (purity 99.7 wt.%), nickel (purity 99.9 wt.%) and zirconium (purity 99.8 wt.%), totaling about 120 g, were melted and remelted at least six times in an argon atmosphere. A

* Corresponding author. Tel.: +886 2 2363 7846; fax: +886 2 2363 4562.
E-mail address: skw@ntu.edu.tw (S.K. Wu).

0925-8388/$ – see front matter © 2005 Elsevier B.V. All rights reserved.
doi:10.1016/j.jallcom.2005.04.193

pure titanium button was used as a getter during the arc melting, and the mass loss during melting was negligibly small. The as-melted ingots were homogenized at 950 °C for 72 h and then quenched in water. They were swaged at 800 °C and then annealed at 850 °C ×1 h. Specimens were cut into several plates with a low speed diamond saw, and then annealed at 900 °C for 1 h and finally quenched in water (i.e. as-annealing). After the annealing, two experimental procedures were conducted. First, some plates were sealed in evacuated quartz tubes and aged at 300 °C for 1–240 h and then quenched in water. Second, some plates were cold-rolled at room temperature to 5% reduction in thickness. Specimens for differential scanning calorimetry (DSC) measurement, IF test, hardness test and microstructure observation were carefully cut from plates treated by the above procedures. The specimen size for the IF test was 110 mm × 4 mm × 1 mm.

Martensitic transformation temperatures were measured using TA Q10 DSC equipment with controlled heating and cooling runs on samples encapsulated in an aluminum pan. The running temperature range was from −100 to +200 °C with the heating and cooling rate of 10 °C/min. The IF test was carried out with a SINKU-RIKO 1500M/L series inverted torsion pendulum in the temperature range from −150 to +250 °C. The tests started from −150 °C, heating up to +250 °C and then cooling down to −150 °C again. Cold-rolled specimens were heated again to +250 °C. The specimens' heating and cooling rate was precisely controlled at 2 °C/min and the test frequency was set at approximately 1 Hz. The testing strain amplitude was kept at 4.5×10^{-5}. The recording of the data was completely automatic; calculation and plots of IF Q^{-1} and frequency f (shear modulus) versus temperature were performed on a digital computer. Thus, experimental results with a rather good resolution were obtained. Specimens for the hardness test were first mechanically polished and then subjected to measurement in a micro-Vickers hardness tester with a 500 g load at room temperature. For each specimen, the average hardness value was taken from at least five test readings. The microstructure observations were made by transmission electron microscope (TEM) with a JEOL-4000FX microscope equipped with a conventional double-tilting stage. The TEM specimens were prepared by electropolishing at −10 °C with an electrolyte consisting of 20% H_2SO_4 and 80% CH_3OH by volume. The applied voltage for electropolishing was 20 V.

3. Experimental results

3.1. Transformation behavior in $Ti_{40.5}Ni_{49.5}Zr_{10}$ alloy

Fig. 1(a and b) show the DSC results of the $Ti_{40.5}Ni_{49.5}Zr_{10}$ alloy as-annealed and aged at 300 °C for 240 h, respectively, in both forward and reverse transformations. The M^* and A^* peaks appearing in Fig. 1 are associated with the first-order martensitic transformation of

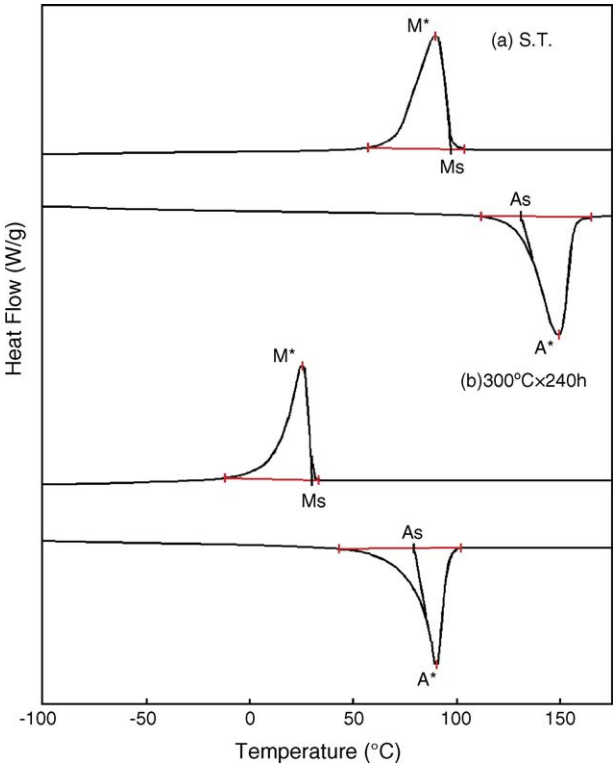

Fig. 1. DSC curve for the annealed $Ti_{40.5}Ni_{49.5}Zr_{10}$ alloy aging at 300 °C for (a) 0 h; S.T. and (b) 240 h.

B2 ↔ B19′ [2]. Here, B2 is the parent phase and B19′ is the monoclinic martensite. In Fig. 1, the transformations exhibit an asymmetric shape of the heat flow peak, i.e. sharp from the high-temperature side and smooth from the low-temperature one. This behavior can be explained by the fact that the stored elastic energy associated with martensitic transformation increases with increasing the volume fraction of the martensite and retards the forward transformation. During the reverse process, the stored elastic energy is released in a reversible manner. Similar behavior is also observed in a $Ni_{42.5}Mn_{50}Ti_{7.5}$ SMA [10]. The temperature difference ΔT between A^* and M^*, as shown in Fig. 1(a), is approximately 62 °C for as-annealed $Ti_{40.5}Ni_{49.5}Zr_{10}$ alloy, which is larger than that for as-annealed $Ti_{51}Ni_{49}$ alloy ($\Delta T = 43$ °C) [11]. This feature indicates that the Zr atoms solid-soluted in Ti-rich TiNi alloy will widen the transformation hysteresis. Fig. 2(a and b) show the plots of f and IF Q^{-1} versus temperature of the as-annealed $Ti_{40.5}Ni_{49.5}Zr_{10}$ alloy, respectively. The full width half-maximum, W, is the temperature range at the half maximum IF peak, as shown in Fig. 2(b). In this figure, there is one peak P_{C1} at 84 °C on the first cooling and one peak P_{H1-1} at 150 °C on the first heating. Both peaks corresponding to the f minimum, as shown in Fig. 2(a), indicating that they are the minima of shear modulus. The peak P_R appearing at −37 °C that does not correspond to the minimum of f is a relaxation peak, which has been observed at −70 °C in the cold-rolled TiNi binary SMAs [12,13].

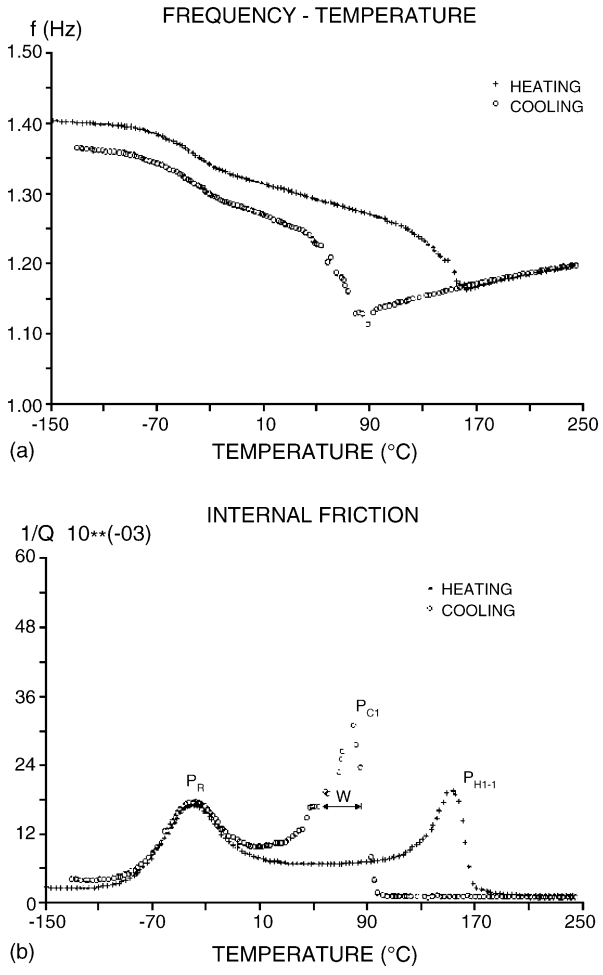

Fig. 2. (a) Frequency, f, and (b) internal friction, Q^{-1}_{max}, vs. temperature for the annealed $Ti_{40.5}Ni_{49.5}Zr_{10}$ alloy. Peaks P_{H1-1} and P_{C1} are associated with the martensitic transformation and peak P_R is a relaxation one.

3.2. Effects of aging on $Ti_{40.5}Ni_{49.5}Zr_{10}$ alloy

Fig. 3(a and b) show the same plots as Fig. 2(a and b), but now for the specimen aged at 300 °C for 240 h. In Fig. 3(b), there is one peak P_{C1} on cooling and one peak P_{H1-1} on heating in the first cycle. Peaks P_{C1} and P_{H1-1} are associated with B2 ↔ B19′ martensitic transformation. A well-shaped relaxation peak P_R appears at −26 °C, as shown in Fig. 3(b). The plots of f and Q^{-1} versus temperature for specimens aged at different time are similar to those of Figs. 2 and 3, except that the transformation temperatures P_{C1}, P_{H1-1}, P_R and their magnitudes of Q^{-1}_{max} and W are different, and thus are omitted here. Fig. 4 shows the Q^{-1}_{max} of peaks P_{C1} and P_{H1-1} versus the aging time which are measured from the IF test. From Fig. 4, the Q^{-1}_{max} of peaks P_{C1} and P_{H1-1} increases with increasing aging time, although transformation temperatures of P_{C1} and P_{H1-1} decrease with increasing aging time [14]. The transformation temperatures also shift to lower values in aged $Ti_{32.3}Ni_{50}Hf_{17.7}$ alloy than in the as-annealed one [15].

Fig. 5(a and b) show the TEM bright-field images of the martensite in specimen as-annealed and that aged at

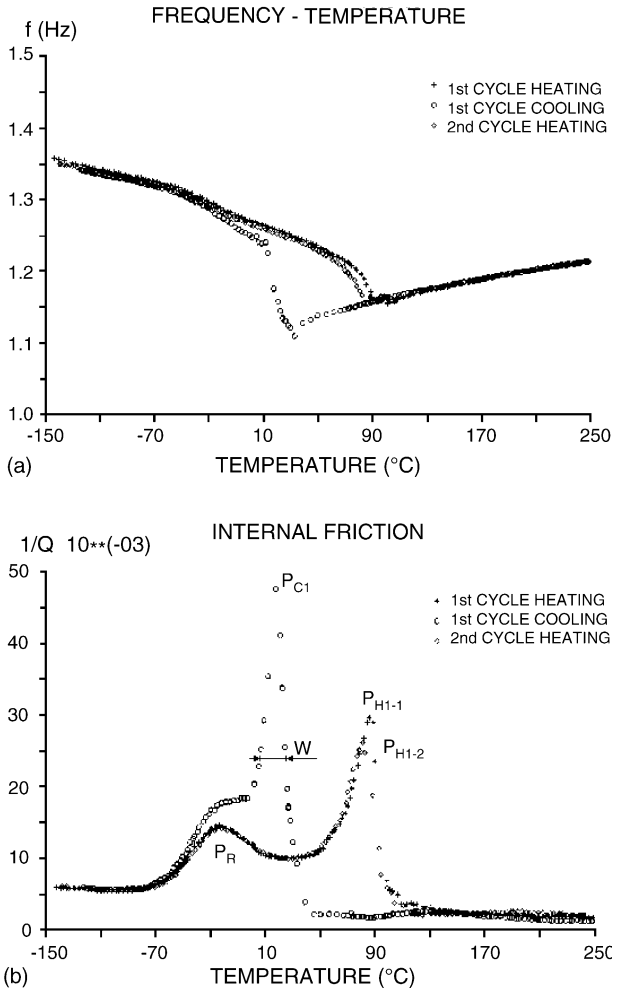

Fig. 3. (a) Frequency, f, and (b) internal friction, Q^{-1}_{max}, vs. temperature for the annealed $Ti_{40.5}Ni_{49.5}Zr_{10}$ alloy aging at 300 °C for 240 h. Peaks P_{H1-1} and P_{C1} are associated with the martensitic transformation and peak P_R is a relaxation one.

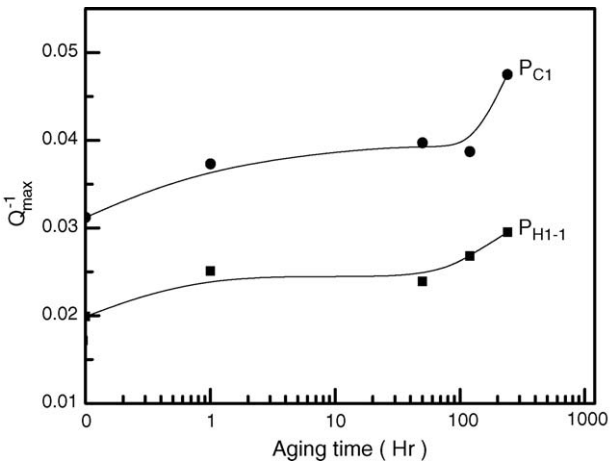

Fig. 4. The IF peak, Q^{-1}_{max}, of P_{H1-1} and P_{C1} vs. aging time for annealed $Ti_{40.5}Ni_{49.5}Zr_{10}$ alloy aged at 300 °C.

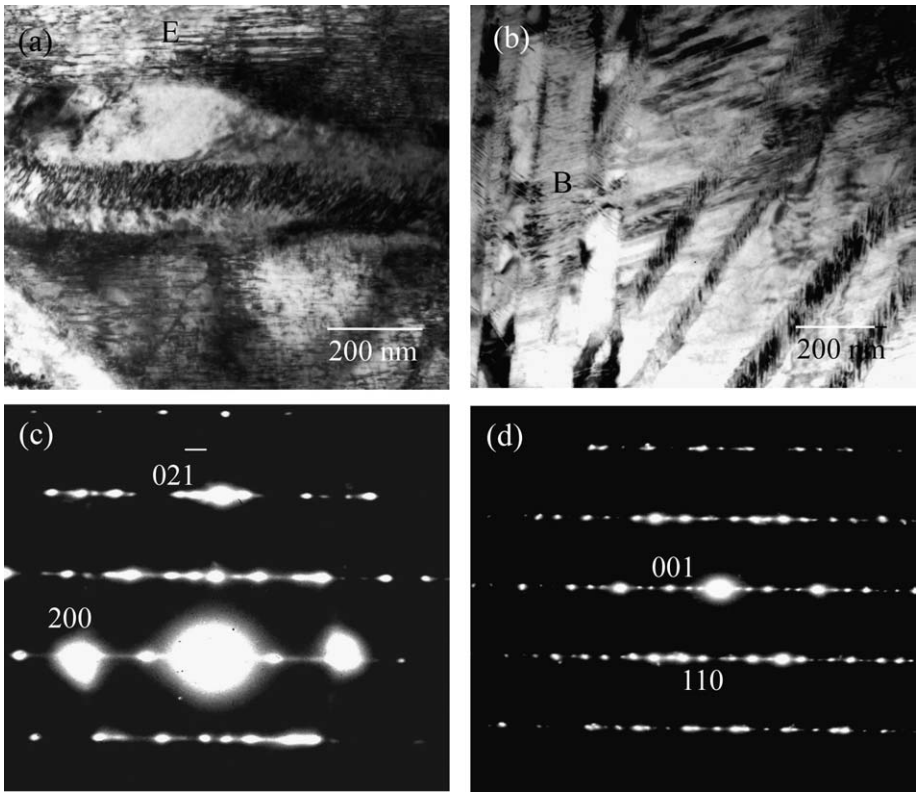

Fig. 5. TEM bright-field image of annealed $Ti_{40.5}Ni_{49.5}Zr_{10}$ alloy aged at 300 °C for (a) 0 h (b) 240 h, SADP taken from areas E and B in (a) and (b), showing $(1\,0\,0)_M$ and $(0\,0\,1)_M$ compound twins with (c) $[0\,\bar{1}\,\bar{2}]_M$ zone axis and (d) $[1\,1\,0]_M$ zone axis, respectively.

300 °C ×240 h, respectively. Fig. 5(c) shows the selected area diffraction pattern (SADP) taken from the martensite plate with fine striations at area E of Fig. 5(a), in which the foil normal is parallel to $[0\,\bar{1}\,\bar{2}]_M$ direction. No extra reflection spots can be observed in Fig. 5(c) except the $(1\,0\,0)_M$ twins. Therefore, the fine striations are the traces of $(1\,0\,0)_M$ twin plates. Based on Han et al. [16], the $[0\,1\,1]_M$ type II twins and $(1\,0\,0)_M$ twins are the main substructures of the martensite in annealed $Ti_{36.5}Ni_{48.5}Hf_{15}$ alloy and there are many defects such as dislocations and microtwins in twin plates. From Fig. 5, $(0\,0\,1)_M$ compound twins are found to exist in $Ti_{40.5}Ni_{49.5}Zr_{10}$ alloy aged at 300 °C for 240 h, as shown in Fig. 5(b) with SADP shown in Fig. 5(d). Compared with Fig. 5(a and b), the abundant fine $(1\,0\,0)_M$ twin plates are observed in the as-annealed specimen, and fine $(0\,0\,1)_M$ twin plates are observed in long aged specimens.

3.3. The effects of light cold-rolling on $Ti_{40.5}Ni_{49.5}Zr_{10}$ alloy

Fig. 6(a and b) show the plots of f and Q^{-1} versus temperature for 5% cold-rolled $Ti_{40.5}Ni_{49.5}Zr_{10}$ alloy, respectively, and peaks P_{H1-1} (191 °C), P_{C1} (64 °C) and P_{H1-2} (133 °C) are all associated with B2↔B19′ martensitic transformation. Peak P_R appearing at −40 °C that does not correspond to the f minima of Fig. 6(a) is a relaxation peak. Mechanically induced martensite stabilization was reported in the cold-rolled $Ti_{50}Ni_{50}$ alloy and the difference between P_{H1-1} and P_{H1-2}, ΔP_H, stands for the degree of martensite stabilization [17]. Similar behavior also occurs in this alloy. The ΔP_H of $Ti_{40.5}Ni_{49.5}Zr_{10}$ alloy shown in Fig. 6 is 58 °C, which is larger than that of $Ti_{50}Ni_{50}$ alloy (ΔP_H = 27 °C) for the same 5% cold-rolling [17]. The increment of the hardness for the 5% cold-rolled specimen is ΔHv = 47 for the former, which is larger than that of the latter (ΔHv = 25). This feature comes from the fact that the as-annealed $Ti_{40.5}Ni_{49.5}Zr_{10}$ alloy (Hv = 273) is harder than the as-annealed $Ti_{50}Ni_{50}$ alloy (Hv = 200) due to Zr atoms solid-soluted hardening in the former. We propose that the dislocation/defect movement associated with twin plate mobility may be impeded more in $Ti_{40.5}Ni_{49.5}Zr_{10}$ alloy than in $Ti_{50}Ni_{50}$ alloy, which causes the harder $Ti_{40.5}Ni_{49.5}Zr_{10}$ alloy to have a higher martensite stabilization under the same degree of cold-rolling.

4. Discussion

4.1. Damping capacity of B2 and B19′ in $Ti_{40.5}Ni_{49.5}Zr_{10}$ alloy

It is well known that there are abundant twin boundaries in B19′ martensite and R phase premartensite of TiNi

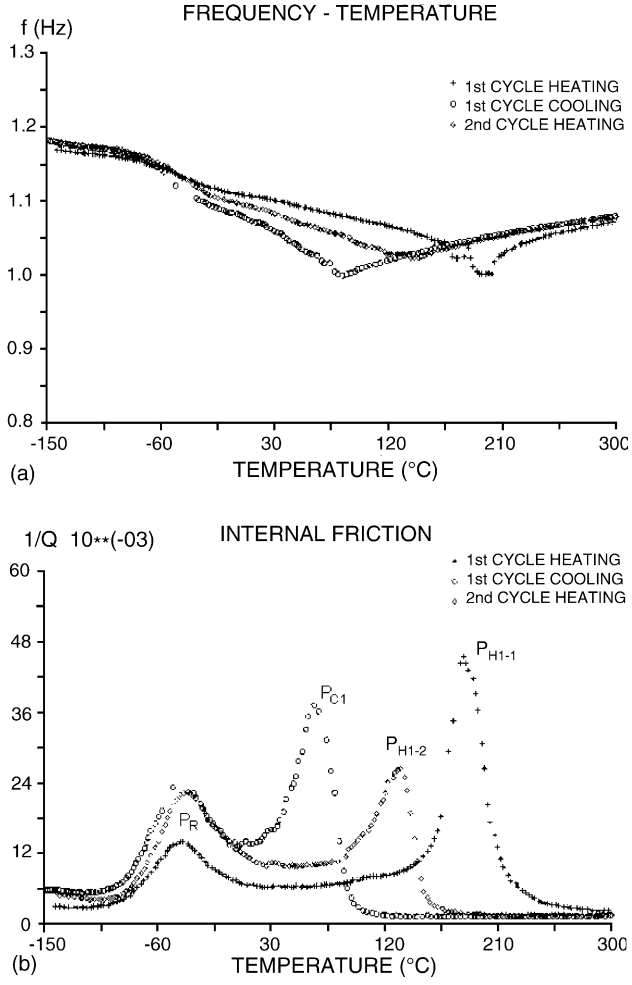

Fig. 6. (a) Frequency, f, and (b) internal friction, Q^{-1}_{max}, vs. temperature for the 5% thickness-reduced $Ti_{40.5}Ni_{49.5}Zr_{10}$ alloy with specimen thickness 1.05 mm. Peaks P_{H1}, and P_{C1} and P_{H1-2} are associated with the martensitic transformation and peak P_R is a relaxation one.

SMAs [18,19]. These twin boundaries can be easily moved by the external stress to accommodate the strain. This phenomenon is the well known "accommodation/reorientation process" occurring in the martensite and R phase of the deformed TiNi alloys. No twin boundaries exist in the B2 parent phase of TiNi alloys [20]. From Fig. 1, $Ti_{40.5}Ni_{49.5}Zr_{10}$ alloy exhibits the thermoelastic B2 ↔ B19′ transformation and the aforementioned behaviors can also occur in this alloy. Hence, in $Ti_{40.5}Ni_{49.5}Zr_{10}$ alloy, the damping capacity of the B2 parent phase is suggested to come simply from the dynamic/static hysteresis of lattice defects, which is smaller than that of B19′ martensite because the dynamic/static hysteresis loop generally dissipates less energy than the accommodation/reorientation process of twin boundaries, as shown in Fig. 2(b).

Lotkov et al. [21] and Mercier et al. [22] investigated the anomalies of elastic properties of TiNi binary and ternary SMAs. They reported that the lattice-softening phenomenon promotes the shear transformation due to the thermal or mechanical driving forces and forms a minimum yield stress around the Ms temperature. This means that, during the martensitic transformation, the movement of twin boundaries or martensite/parent interfaces is easy and most of the energy is dissipated in the transformation region. The damping capacity of B19′ martensite for ternary $Ti_{50}Ni_{49.5}Fe_{0.5}$ and $Ti_{50}Ni_{40}Cu_{10}$ alloys is higher than that for $Ti_{50}Ni_{50}$ alloy because the former two alloys have the lower yield stress and shear modulus [23]. Compared with Fig. 2 and Ref. [11], the f (shear modulus) of B19′ and B2 phases of $Ti_{40.5}Ni_{49.5}Zr_{10}$ alloy is larger than that of $Ti_{51}Ni_{49}$ alloy, where the IF peak ($Q^{-1}_{max} = 3.12 \times 10^{-2}$ at P_{Cl}) of the former is lower than that of the latter ($Q^{-1}_{max} = 5.2 \times 10^{-2}$ at P_{Cl}) with the same specimen size. This feature exhibits the Zr atoms solid-soluted hardening in $Ti_{40.5}Ni_{49.5}Zr_{10}$ alloy and decreasing the mobility of twin plates in martensite and/or that of interfaces between martensite and parent phase. Therefore, damping capacities of B19′ and B2 phases of $Ti_{40.5}Ni_{49.5}Zr_{10}$ alloy are lower than those of $Ti_{51}Ni_{49}$ alloy.

4.2. Internal friction in aged $Ti_{40.5}Ni_{49.5}Zr_{10}$ alloy

Delorme et al. [24] indicated that all the first-order phase transformations should be accompanied by IF peaks and they deduced the Q^{-1} as a function of temperature changing rate dT/dt, as shown in Eq. (1):

$$Q^{-1} = \frac{1}{\omega}\frac{d\psi(V_m)}{dV_m}\frac{dV_m}{dT}\frac{dT}{dt} \quad (1)$$

where V_m is the volume fraction of the martensite, ω the angular frequency of the applied stress and $\Psi(V_m)$ is a monotonic function associated with the transformation change and/or shape strain. Eq. (1) indicates that the Q^{-1} is proportional to the heating and cooling rate, dT/dt. Dejonghe et al. [25], in order to take account of the special character of a martensite that can be induced or reoriented by an external stress σ, introduced the stress dependence to dV_m/dt as follows:

$$\frac{dV_m}{dt} = \frac{\partial V_m}{\partial T}\frac{\partial T}{\partial t} + \frac{\partial V_m}{\partial \sigma}\frac{\partial \sigma}{\partial t} \quad (2)$$

In Eq. (2), the first-term is identical to the Delorme's model and the second-term is stress-dependent. From Delorme's model [24], supposing $d\Psi(V_m)/dV_m$ remains constant for all thermoelastic martensites and keeping the angular frequency and the cooling or heating rate as constants in this study, the Q^{-1}_{max} should be proportional to the mount of martensite formed per unit temperature or time (dV_m/dT or dV_m/dt). From Figs. 2 and 3, we find that Q^{-1}_{max} values of martensitic transformations P_{C1} and P_{H1-1} of $Ti_{40.5}Ni_{49.5}Zr_{10}$ specimen aged at 300 °C for 240 h are higher than those of the as-annealed one, but the W width of the former is smaller than the latter. This result shows that the aged $Ti_{40.5}Ni_{49.5}Zr_{10}$ alloy can enhance the martensite formation per unit temperature or time. It is well known that the mechanical energy dissipation of the martensite should depend on its twin type of TiNi SMAs. The most frequently observed twinning mode in TiNi

binary alloys is the ⟨0 1 1⟩ type II twin [26] which is also their lattice invariant shear (LIS). However, it has been proved that the (0 0 1) compound twin is the LIS of $Ti_{42.2}Ni_{49.8}Hf_8$ and $Ti_{36.5}Ni_{48.5}Hf_{15}$ alloys [3,27]. From Fig. 5, the $(0\,0\,1)_M$ twin planes are more dense in the 300 °C ×240 h aged specimen, but $(1\,0\,0)_M$ twin planes are more dense in the as-annealed one. These results indicate that the ⟨0 1 1⟩ type II and $(1\,0\,0)_M$ twins can evolve to $(0\,0\,1)_M$ twins in the aged $Ti_{40.5}Ni_{49.5}Zr_{10}$ alloy. Hence, the higher peak Q^{-1}_{max} and the smaller width W of the longer aged $Ti_{40.5}Ni_{49.5}Zr_{10}$ specimen are attributable to stress-assisted twin-boundary motions of the abundant $(0\,0\,1)_M$ twins. The behaviors of these IF peaks associated with martensitic transformation agree with Delorme's model.

The asymmetric transformation peaks of IF test shown in Figs. 2(b) and 3(b) are similar to those of the DSC measurement shown in Fig. 1(a and b). We propose that the IF peaks smoothing from low-temperature side are closely related to the stored elastic energy associated with martensitic transformation, which is the same reason for the asymmetric DSC peaks discussed in Section 3.1.

4.3. Internal friction in cold-rolled $Ti_{40.5}Ni_{49.5}Zr_{10}$ alloy

Based on the vibration theory [28], the reduction in the specimen thickness will decrease the natural frequency of the specimen under the same amplitude when the specimen's length and width are kept constant. Therefore, the frequency f should decrease when the specimen is slightly cold-rolled (5% thickness reduction), as compared with Figs. 2(a) and 6(a). At the same time, the IF peak Q^{-1}_{max} of the 5% cold-rolled specimen is higher than that of the as-annealed one. Lin et al. [17] reported that the light cold-rolling (≤5% thickness reduction) of $Ti_{50}Ni_{50}$ binary alloy increases the Q^{-1}_{max} of transformation peaks. Dalle et al. [3] reported that $(0\,0\,1)_M$ twinning in the 6.7% deformed $Ti_{42.2}Ni_{49.8}Hf_8$ specimen is thinner than that in the undeformed one, where the small deformation is accommodated by $(0\,0\,1)_M$ twinning and the further deformation is accommodated by the detwinning of these micro-twins. We suggest that the same phenomenon can also be found in the slightly cold-rolled $Ti_{40.5}Ni_{49.5}Zr_{10}$ alloy. Hence, the higher Q^{-1}_{max} of the slightly cold-rolled $Ti_{40.5}Ni_{49.5}Zr_{10}$ alloy shown in Fig. 6(b) than that of the as-annealed alloy shown in Fig. 2(b) is attributable to the thinner $(0\,0\,1)_M$ twins induced by small deformation, which are suggested to be easier to accommodate.

5. Conclusion

1. The as-annealed $Ti_{40.5}Ni_{49.5}Zr_{10}$ alloy undergoes one-stage B2 ↔ B19′ martensitic transformation. Damping capacities of B19′ and B2 phases of this alloy are lower than those of $Ti_{51}Ni_{49}$ alloy due to Zr atoms solid-soluted hardening.
2. With increasing aging time at 300 °C, the transformation peak height Q^{-1}_{max} increases, but transformation temperature decreases. These characteristics are closely related to the aging effects on the formation of finer $(0\,0\,1)_M$ twins for specimens aged longer.
3. The degree of martensite stabilization of $Ti_{40.5}Ni_{49.5}Zr_{10}$ alloy is larger than that of $Ti_{50}Ni_{50}$ alloy for the same 5% cold-rolling because the former has a higher inherent hardness than the latter. The higher peak Q^{-1}_{max} of the slightly deformed $Ti_{40.5}Ni_{49.5}Zr_{10}$ alloy compared to the as-annealed one is attributable to the thinner $(0\,0\,1)_M$ twins induced by small deformation.

Acknowledgements

The authors are pleased to acknowledge the financial support of this research by the National Science Council (NSC), Republic of China under Grants NSC 93-2216-E002-003 and NSC 93-2216-E151-017.

References

[1] J.H. Mulder, J.H. Mass, J. Beyer, ICOMAT (1992) 869–874.
[2] S.F. Hsieh, S.K. Wu, J. Alloys Compd. 266 (1998) 276–282.
[3] F. Dalle, E. Perrin, P. Vermaut, M. Masse, R. Portier, Acta Mater. 50 (2002) 3557–3565.
[4] O. Mercier, K.N. Melton, Y. De Preville, Acta Metall. 27 (1979) 1467–1475.
[5] I.G. Ritchie, Z.-L. Pan, Metall. Trans. 22A (1991) 607–616.
[6] R. De Batist, Internal Friction of Structural Defects in Crystalline Solids, North-Holland Publishing Co., Amsterdam, 1972.
[7] D.W. James, Mater. Sci. Eng. 4 (1969) 1–8.
[8] R. De Batist, J. Phys. (1983) C9–C39.
[9] J. Van Humbeck, Proceedings of The ASM Materials Week and TMS/AIME Fall Meeting, Role of Interfaces on Materials Damping, ASM, Materials Park, OH, 1985, pp. 5–24.
[10] P.L. Potapov, R. Gotthardt, L. Bataillard, Phys. Stat. Sol. 165 (1998) 401–408.
[11] H.C. Lin, S.K. Wu, J.C. Lin, Mater. Chem. Phys. 37 (1994) 184–190.
[12] K. Iwasaki, R. Hasiguti, Trans. JIM 28 (1987) 363–367.
[13] H.C. Lin, S.K. Wu, T.S. Chou, J. Alloys Compd. 355 (2003) 90–96.
[14] S.F. Hsieh, S.K. Wu, J. Alloys Compd. 270 (1998) 237–241.
[15] R. Santamarta, C. Segui, J. Pons, E. Cesari, Scr. Mater. 41 (1999) 867–872.
[16] X.D. Han, W.H. Zou, R. Wang, Z. Zhang, D.Z. Yang, K.H. Wu, J. De Phys. IV (1995), C8-73-C758.
[17] H.C. Lin, S.K. Wu, T.S. Chou, H.P. Kao, Acta Metall. 39 (1991) 2069–2080.
[18] T. Onda, Y. Bando, T. Ohba, K. Otsuka, Mater. Trans., JIM 33 (1992) 354–359.
[19] S. Miyazaki, C.M. Wayman, Acta Metall. 36 (1988) 181–192.
[20] H.C. Lin, S.K. Wu, M.T. Yeh, Metall. Trans. 24A (1993) 2189–2194.
[21] A.I. Lotkov, A.V. Kuznetsov, V.N. Griskov, A.A. Botaki, in: Y. Chu, T.Y. Hsu, T. Ko (Eds.), Proceedings of International Shape Memory Alloy Symposium, China Academic Publishers, Guilin, China, 1986, pp. 153–158.

[22] O. Mercier, K.N. Melton, G. Gremaud, J. Hagi, J. Appl. Phys. 41 (1980) 1833–1834.
[23] H.C. Lin, S.K. Wu, Y.C. Chang, Metall. Trans. 26A (1995) 851–858.
[24] J.F. Delorme, R. Schmid, M. Robin, P. Gobin, J. Phys. C2 (1971) 101–109.
[25] W. Dejonghe, R. de Batist, L. Delaey, Scr. Metall. 10 (1976) 1125–1128.
[26] M. Nishida, H. Ohgi, I. Itai, A. Chiba, K. Yamauchi, Acta Mater. 43 (1995) 1229–1234.
[27] X.D. Han, W.H. Zou, R. Wang, Z. Zhang, D.Z. Yang, Acta Mater. 44 (1996) 3711–3721.
[28] B.H. Tongue, Principles of Vibration, second ed., Oxford University Press, Oxford, 2002, pp. 17–18.